



HAL
open science

Numerical modeling of powder spreading in additive manufacturing processes: effects of process parameters and particle size distribution

Alexis Burr, Maxime Stephan, Mathieu Soulier

► To cite this version:

Alexis Burr, Maxime Stephan, Mathieu Soulier. Numerical modeling of powder spreading in additive manufacturing processes: effects of process parameters and particle size distribution. Word PM2022 - Tools for improving PM, European Powder Metallurgy Association (EPMA), Oct 2022, Lyon, France. pp.5370331. cea-03843322

HAL Id: cea-03843322

<https://cea.hal.science/cea-03843322>

Submitted on 8 Nov 2022

HAL is a multi-disciplinary open access archive for the deposit and dissemination of scientific research documents, whether they are published or not. The documents may come from teaching and research institutions in France or abroad, or from public or private research centers.

L'archive ouverte pluridisciplinaire **HAL**, est destinée au dépôt et à la diffusion de documents scientifiques de niveau recherche, publiés ou non, émanant des établissements d'enseignement et de recherche français ou étrangers, des laboratoires publics ou privés.

Numerical modeling of powder spreading in additive manufacturing processes: effects of process parameters and particle size distribution

A. Burr alexis.burr@cea.fr, M. Stephan, M. Soulier

Univ. Grenoble Alpes, CEA-LITEN, F-38000 Grenoble

Abstract:

Powder bed properties are of main interests in additive manufacturing processes. Particularly, it is paramount to ensure a correct density of the powder bed as this will have an impact on the final part properties. In this work, we propose to model the deposition of powder by the discrete element method through an elastic contact law (using the EDEM software from Altair with GPU acceleration). Different particle size distributions are used with different recoating strategies so as to estimate the effect of the mean particle size, recoater speed and nominal layer thickness on the powder bed density and segregation. Those two quantities evolve similarly with the increase of layer thickness, whatever the particle size distribution. Only the segregation is observed to have a larger impact for wider particle size distribution.

Introduction:

Powder bed based additive manufacturing processes such as laser powder bed fusion (L-PBF) and binder jetting (BJ) rely on the successive recoating of powder layers one over the another. The deposited material is then consolidated either by melting or thanks to a binder. However, the state of the powder before consolidation, e.g. its relative density, is paramount for a dense and mechanically strong final part [1]–[3]. Understanding and predicting the spreadability of a powder depending on its specifications and on the process parameters has recently gained a strong interest by the powder metallurgy community. Some experimental test benches have been developed [4] [5], but much more numerical investigations were performed using the discrete element methods. Studies focused on determining the impact of various parameters on powder bed quality, which is usually defined by the powder bed relative density and surface roughness. For a given layer thickness, small particle size tends to give larger relative densities as long as the cohesiveness is small [6], [7]. The shape of particles also has an influence with elongated particles leading to larger bed roughness and generally decreases the relative density [8]. The surface energy was found to be a first order parameter which decreases the powder bed quality with increasing values [6], [7], [9], [10]. It is a troublesome parameter as its determination is usually done by comparing experimental and numerical angle of repose tests [11], [12]. A scale law is required to fit numerical to experimental data [13], [14]. Particle size distribution has also been investigated to narrow the range of appropriate powder for spreading [12], [15]. Regarding the process parameters, it was well demonstrated that decreasing the layer thickness with respect to the particle size, or increasing the recoating velocity, will both be detrimental for the powder bed quality, decreasing the relative density, possibly jamming particles, and increasing the roughness [7], [15]–[18]. Finally, the recoater geometry is still an open debate, and the discrete element simulations is a step forward to optimize it without trial-and-errors [19]–[21].

Most studies focused on the first deposited layer of powder. In this work, we compare such deposition to a configuration in which the powder is recoated on previous layers. We take advantage of a GPU-accelerated code to model several hundreds of thousands of small particles in a reasonable time frame. We propose to compare both configurations for four different particle size distributions and two velocities of the blade and then to assess impacts on the powder bed relative density, segregation and surface height.

Methods:

In the discrete element method, rigid particles (representing powder grains) are interacting each other through contact laws. In this work, particles are spherical, and are defined by their position and diameter. When two particles are in contact, an elastic repulsion is assumed in this work, with a damping by using the Hertz-Mindlin model, while adhesion is intentionally overlooked. The EDEM [22] code edited by Altair is used to perform discrete element simulations using GPU-acceleration.

Two configurations of the simulated geometry are proposed in Figure 1. Configuration A could be a representation of the powder spreading of the first layer in L-PBF, or on the previously melted layer,

while configuration B is more representative of the system in Metal Binder Jetting, for which a thick amount of powder is already deposited before any printing. In configuration A, the powder is directly deposited on the building platform in one pass. The layer thickness h_0 ranges from $2D_{50}$ to $5D_{50}$ (determined in number). In configuration B, the powder is generated on the loading platform, and a first layer of $500\ \mu\text{m}$ is spread on the building platform. Then, the loading platform goes up, the building platform goes down by an increment of D_{50} or $2D_{50}$ before a second layer is spread on the first thick layer. The blade stays at the same altitude of $500\ \mu\text{m}$ between the two layers. Moreover, the building platform as well as the blade are $10\ \text{mm}$ long in both configurations. The blade is supposed to be rubber-blade, while other parts are in stainless steel.

Two velocities of 50 and $100\ \text{mm/s}$ are used for the simulations. Table 1 gives a summary of the different tested parameters.

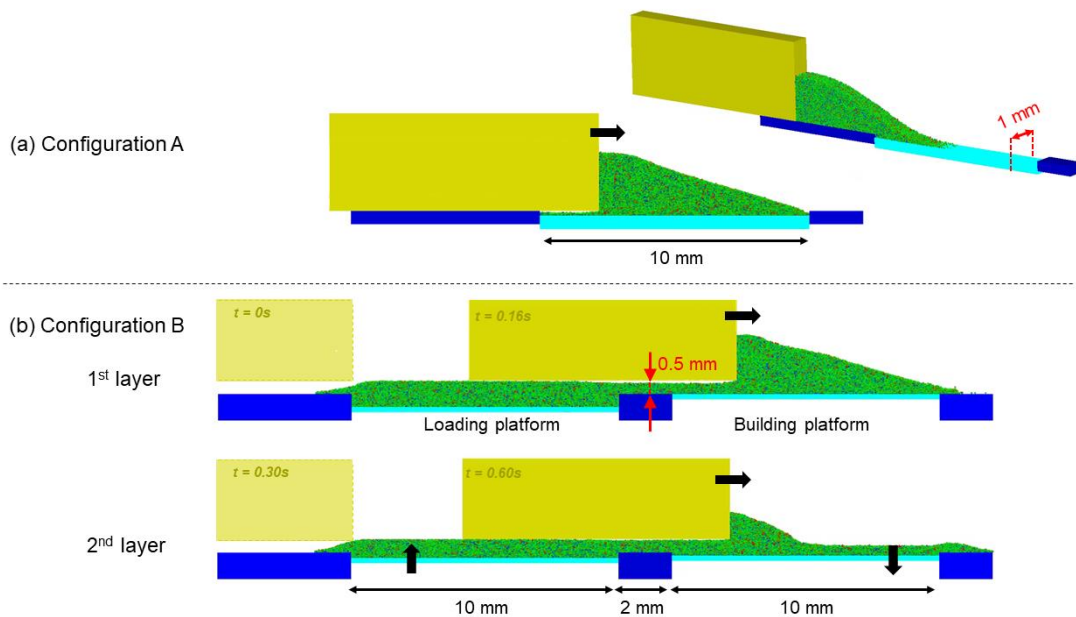


Figure 1 : Two configurations of the geometry for the deposition of powder. Configuration A spread the powder directly on the building platform, while configuration B spread the powder on an already existing layer.

Parameters	Values	Parameters	Values
Young modulus	$2.10^7\ \text{Pa}$	Coefficient of restitution particle-particle/wall	0.4
Poisson's ratio	0.3	Coefficient of restitution particle-blade	0.95
Density	$7960\ \text{kg.m}^{-3}$	Coefficient of static friction particle-particle/wall	0.4
Coefficient of rolling friction	0.01	Coefficient of static friction particle-blade	0.8

Table 1: Parameters used for the discrete simulations

Four particle size distributions (PSD) are used and compared in this work. Figure 2a-b depicts that the histograms of the chosen distributions are lognormal. Distribution α is a fit on the real distribution of a 316L stainless steel powder that was studied experimentally on a powder spreading test bench [5]. Distribution β has the same median diameter but a standard deviation twice smaller in a logarithmic scale. Similarly, the median diameter of distributions γ and ω is twice the one of α , and their standard deviation are identical or multiplied by 2 in a logarithmic scale. All distributions are represented using number of particles instead of volumes, for comparison purposes.

Only the powder deposited on the building platform is analyzed in this work. Therefore, in configuration B, a rectangular subvolume of 10 mm length, 1mm side and of the layer height is extracted from the simulation results. Figure 2c illustrates how the subvolume is divided in 10 bins of 1x1 mm (XY). The relative density is averaged in each of those bins using the nominal layer height h_0 , while the D_{10} , D_{50} and D_{90} are also extracted. In this work, only the normalized bed height is proposed to describe the powder bed surface. It is the ratio between the deposited height h by the nominal one h_0 . To determine the density and the surface height, a routine was written to voxelize the powder bed in a 3D image. Then, calculations are done similarly to Meier *et al.* [7].

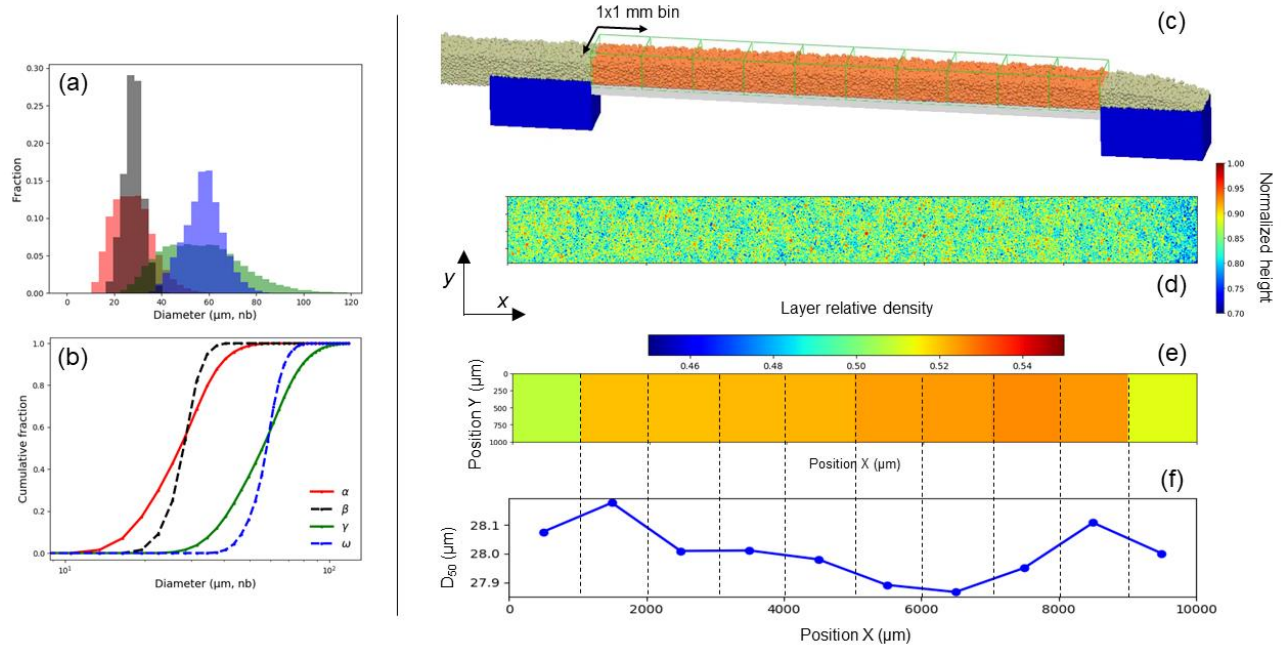


Figure 2: (a) Histograms and (b) cumulative fraction of particle size distributions used in this work. The distributions are lognormal. (c) Extraction of the powder bed subvolume to be analyzed. The surface height to nominal layer height is illustrated in (d). Bottom figures represent the layer relative density (e) and the D_{50} (f) evolution using 10 boxes of 1x1mm size along the spreading direction.

Results and discussion:

Figure 3 depicts that the relative densities are drastically smaller in configuration A than in configuration B. Using a recoating velocity of 100 mm/s leads to worse relative densities than using 50 mm/s whatever the configurations or PSD. The consistent increase of the relative density with the increase of the layer thickness in Figure 3a is known by the “wall-effect” [15]. The mechanisms responsible for those differences are illustrated by particle velocity vectors for the two configurations in Figure 3c and f. It distinctly shows the motion of particles inside the existing powder bed, which helps rearrange particles.

For a layer thickness of $5D_{50}$, the relative density reached is about the same as in configuration B. The relative density always increases near the end of the bed in Figure 3a because of a small pile of powder that forms (see Figure 4). The first layer of 500μm always exhibits relative densities lower than in the second layer, whatever the speed of their deposition. Performing a second layer of D_{50} or $2D_{50}$ increases the density but no great differences are observed depending on the layer thickness by comparison to the effect of the velocity. Note that PSD α shows values of relative density very close to what was experimentally observed [5] for this distribution in configuration B, and that using smaller particles leads to better powder bed relative densities with the used material parameters. The large variability of the density for PSD γ and ω at 100 mm/s with a $2D_{50}$ layer thickness (Figure 3e) can be understood by comparing the normalized height in Figure 4. A small pile of powder forms in the range 8000-9500 μm and a slightly depleted zone appears after it (500μm to the end of the bed) and also at

the very beginning (see Figure 4b and c). The normalized height also suggests that the intended deposited height is never reached but it gets closer to it as the particle size and the blade velocity decrease. Moreover, the normalized height increases as the layer thickness increases, so it is favored by configuration B, and is well correlated to the relative density in configuration A. It decreases with larger blade velocity and typically increases when the size of the particles is small compared to the simulated geometry.

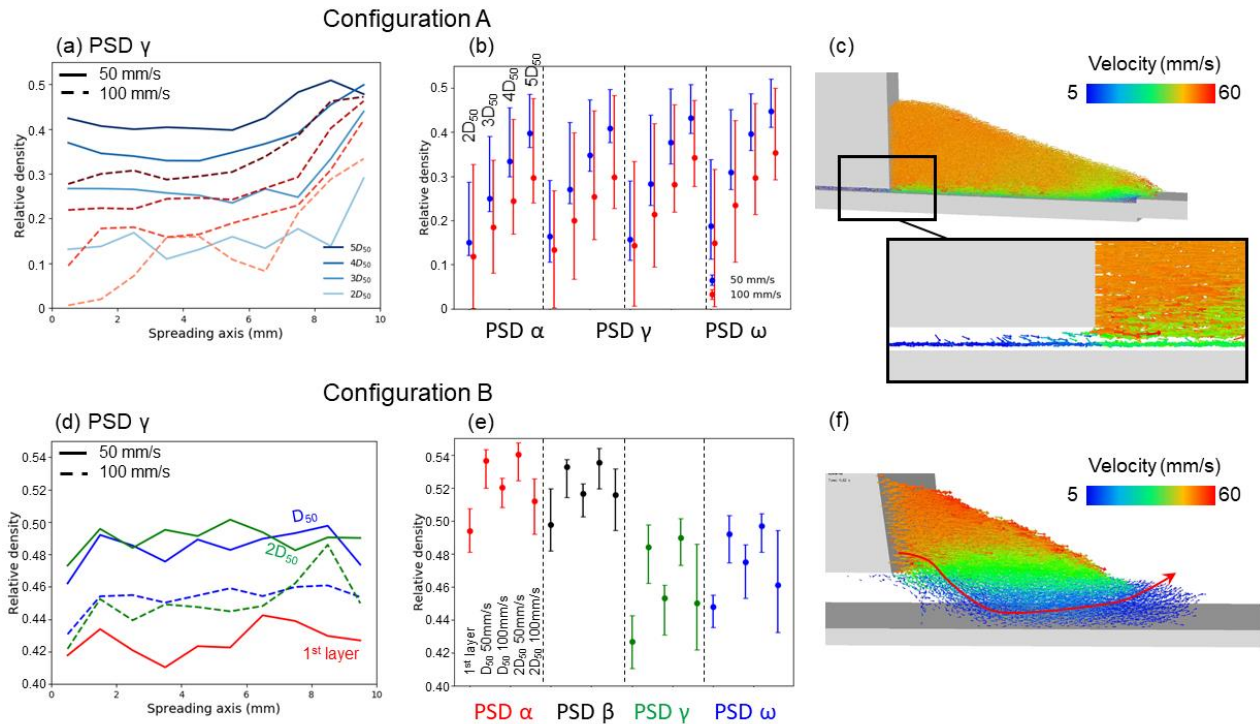


Figure 3: Evolution of the relative density for (a)-(c) configuration A and (d)-(f) configuration B. Only the particle size distribution γ is represented on (a) and (d), whereas all distributions are compared on (b) and (e). For clarity, the errorbars on (b) and (e) ranges from the minimum to the maximum value obtained for the density in the 10 bins along the spreading axis, with the dot giving the mean value.

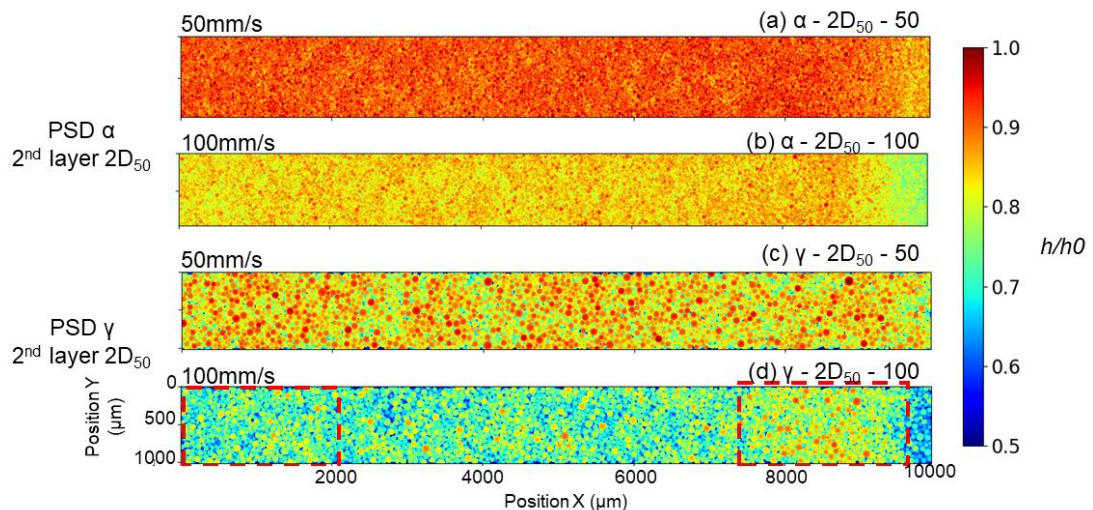


Figure 4: Normalized height (surface height of the powder bed h divided by the nominal height h_0) for configuration B and different spreading. Spreading of a second layer of height $2D_{50}$ for PSD α at velocities (a) 50 mm/s and (b) 100 mm/s. Spreading of a second layer of height $2D_{50}$ for PSD γ at velocities (a) 50 mm/s and (b) 100 mm/s. Red dashed squares highlight the small depletion at the beginning of the bed and the powder pile formed at the end.

The segregation after powder spreading is represented by the D_{50} evolution in Figure 5. Similarly to the relative density, the increase of the layer thickness in configuration A from $2D_{50}$ to $5D_{50}$ leads to an increase of the D_{50} of the powder bed, towards its initial value (see Figure 5a). This means segregation occurs drastically at small layer thickness, with large particles being pushed to the end of the bed.

In Figure 5b, all PSDs results are compiled and they all exhibit a larger segregation for small layer thicknesses. Results for the D_{50} of the bed are always below the D_{50} of the generated powder. Contrary to what was observed for the relative density, the effect of the width of the distribution has a major effect on the segregation results. In fact, with a larger width (i.e. PSD α and γ), results along the spreading axis are more scattered, leading to the larger variabilities observed in Figure 5b,c and d. Those error bars are defined by the minimum and maximum D_{50} values observed in the 10 bins of the powder bed. For instance, the difference of D_{50} in every bin can reach $17\mu\text{m}$ for PSD γ for a recoating at 100 mm/s for a $2D_{50}$ layer thickness, while it only reaches $5.5\mu\text{m}$ for PSD ω and the same process parameters.

Moreover, the change of blade velocity (multiplication by 2) does not lead to distinct difference for the D_{50} of the bed whatever the particle size distribution (Figure 5b). Only the smallest layer thickness (i.e. $2D_{50}$), shows a difference between the minimum and maximum value, greater at 100 mm/s than at 50mm/s .

Therefore, excepting at $2D_{50}$, results suggest no differences for the segregation between the two velocities, contrary to the observations of [12], which concluded a reduction of the segregation thanks to an increase of the velocity. However, those conclusions stemmed out of a much longer simulated powder bed, with slightly different material parameters.

Most observations made for configuration A can be reiterated for results obtained with configuration B (Figure 5c-d). The main difference comes from the range of values obtained for the D_{50} of the powder bed which is much narrower for all PSDs (roughly ΔD_{50} is $< 1\mu\text{m}$ for PSD α , $< 0.25\mu\text{m}$ for PSD β , $< 3\mu\text{m}$ for PSD γ , and $< 1.5\mu\text{m}$ for PSD ω). This means that segregation may not be an issue during the powder deposition in metal binder jetting.

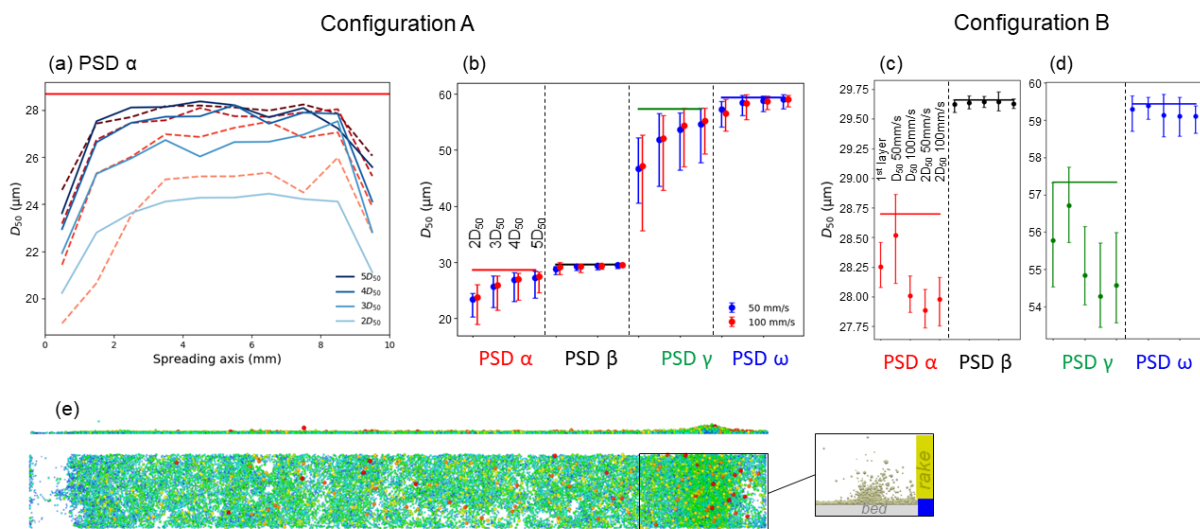


Figure 5: Evolution of the D_{50} for (a)-(b) configuration A and (c)-(d) configuration B. Only the particle size distribution α is represented on (a) for velocities 50 and 100 mm/s , whereas all distributions are compared on (b) and (c-d). Horizontal bars on (a) to (d) gives the value of D_{50} of the generated powder before spreading. For clarity, the error bars on (b-d) ranges from the minimum to the maximum value obtained for D_{50} in the 10 bins along the spreading axis, with the dot giving the mean value. Powder bed view (Figure 5e) illustrates the deposition of PSD α at 100mm/s and the instabilities at the end of spreading (jamming of particles that are suddenly released, leading to powder depletion).

Finally, some features appear especially for a single recoated layer. For instance, particles can be stuck at the end of the bed between the blade, the powder bed and the small step avoiding the powder to fall (see Figure 5e). Once the powder is released, it explodes backwards, leading to a small depletion zone and a small powder pile.

Conclusions:

This work focused on the modelling of powder spreading using the discrete element method. A simple elastic contact law with no adhesion was used to model the contact between particles. Efforts were concentrated on two types of configurations for the powder spreading, that are common in additive manufacturing: the first one consisting of a sole layer directly deposited on the building platform (typical for L-PBF), the second focused on the deposition of a powder layer on a preexisting powder bed (typical for binder jetting). This second type of simulations was possible to perform thanks to GPU-computing, which is helpful for large number of particles (here, more than 600 000 for the smallest D_{50}). The comparison was done by three descriptors: the relative density, the normalized height and the segregation, only depicted here by the D_{50} .

Most results are straightforward: increasing the layer thickness or reducing the particle size leads to an increase of the relative density. Recoating a layer on an already deposited powder bed, will increase the overall density until a maximum is reached. This is due to the possibility of particles of the powder pile to enter in the preexisting bed. On the contrary, depositing a layer directly on a building platform hinders the possibility for particles to rearrange, and a “wall-effect” appears. Similar trends were obtained for the normalized height.

Segregation is also much more pronounced in the case of a single deposited layer. Large variability along the powder bed is observed for particle size distribution with a large width. The D_{50} of the powder bed is also always smaller than the D_{50} of the generated/initial powder but tends to this value with increasing layer thickness. This suggests that large particles are pushed to the end of the powder bed, and therefore to the collecting device. In such case, recoating a powder layer on a preexisting powder bed is also helpful to avoid segregation.

Future work will involve the calibration of material parameters to take into account in particular adhesion effects, which impact is known on spreadability of fine cohesive particles. Furthermore, the segregation was studied only using the D_{50} , while some other quantities could be looked upon, such as the evolution of the span during spreading. Finally, studying the effects of a roller recoater is also of interest as several systems use such device to spread the powder.

References:

- [1] E. Vasquez *et al.*, « Effect of powder characteristics on production of oxide dispersion strengthened Fe 14Cr steel by laser powder bed fusion », *Powder Technology*, vol. 360, p. 998-1005, janv. 2020, doi: 10.1016/j.powtec.2019.11.022.
- [2] M. Ziaee et N. B. Crane, « Binder jetting: A review of process, materials, and methods », *Additive Manufacturing*, vol. 28, p. 781-801, août 2019, doi: 10.1016/j.addma.2019.05.031.
- [3] H. Chen, T. Cheng, Z. Li, Q. Wei, et W. Yan, « Is high-speed powder spreading really unfavourable for the part quality of laser powder bed fusion additive manufacturing? », *Acta Materialia*, vol. 231, p. 117901, juin 2022, doi: 10.1016/j.actamat.2022.117901.
- [4] D. Oropeza, R. Roberts, et A. J. Hart, « A modular testbed for mechanized spreading of powder layers for additive manufacturing », *Review of Scientific Instruments*, vol. 92, n° 1, p. 015114, janv. 2021, doi: 10.1063/5.0031191.
- [5] Mathieu Soulier, Alexis Burr, Nathaël Dubois, Guilhem Roux, Julie Maisonneuve, et Richard Laucournet, « Analytical and Numerical Modelling of Stainless Steel Powders Spreading in Powder-Bed Processes for Additive Manufacturing », 2021.
- [6] Y. He, A. Hassanpour, et A. E. Bayly, « Combined effect of particle size and surface cohesiveness on powder spreadability for additive manufacturing », *Powder Technology*, vol. 392, p. 191-203, nov. 2021, doi: 10.1016/j.powtec.2021.06.046.

- [7] C. Meier, R. Weissbach, J. Weinberg, W. A. Wall, et A. J. Hart, « Critical influences of particle size and adhesion on the powder layer uniformity in metal additive manufacturing », *Journal of Materials Processing Technology*, vol. 266, p. 484-501, avr. 2019, doi: 10.1016/j.jmatprotec.2018.10.037.
- [8] S. Haeri, Y. Wang, O. Ghita, et J. Sun, « Discrete element simulation and experimental study of powder spreading process in additive manufacturing », *Powder Technology*, vol. 306, p. 45-54, janv. 2017, doi: 10.1016/j.powtec.2016.11.002.
- [9] K. Marchais, J. Girardot, C. Metton, et I. Iordanoff, « A 3D DEM simulation to study the influence of material and process parameters on spreading of metallic powder in additive manufacturing », *Comp. Part. Mech.*, janv. 2021, doi: 10.1007/s40571-020-00380-z.
- [10] L. Wang, E. L. Li, H. Shen, R. P. Zou, A. B. Yu, et Z. Y. Zhou, « Adhesion effects on spreading of metal powders in selective laser melting », *Powder Technology*, vol. 363, p. 602-610, mars 2020, doi: 10.1016/j.powtec.2019.12.048.
- [11] C. Meier, R. Weissbach, J. Weinberg, W. A. Wall, et A. John Hart, « Modeling and characterization of cohesion in fine metal powders with a focus on additive manufacturing process simulations », *Powder Technology*, vol. 343, p. 855-866, févr. 2019, doi: 10.1016/j.powtec.2018.11.072.
- [12] D. Yao *et al.*, « Segregation of 316L stainless steel powder during spreading in selective laser melting based additive manufacturing », *Powder Technology*, p. 117096, janv. 2022, doi: 10.1016/j.powtec.2021.117096.
- [13] W. Nan *et al.*, « Jamming during particle spreading in additive manufacturing », *Powder Technology*, vol. 338, p. 253-262, oct. 2018, doi: 10.1016/j.powtec.2018.07.030.
- [14] W. Nan, M. Pasha, et M. Ghadiri, « Numerical simulation of particle flow and segregation during roller spreading process in additive manufacturing », *Powder Technology*, vol. 364, p. 811-821, mars 2020, doi: 10.1016/j.powtec.2019.12.023.
- [15] H. Chen, Q. Wei, Y. Zhang, F. Chen, Y. Shi, et W. Yan, « Powder-spreading mechanisms in powder-bed-based additive manufacturing: Experiments and computational modeling », *Acta Materialia*, vol. 179, p. 158-171, oct. 2019, doi: 10.1016/j.actamat.2019.08.030.
- [16] E. J. R. Parteli et T. Pöschel, « Particle-based simulation of powder application in additive manufacturing », *Powder Technology*, vol. 288, p. 96-102, janv. 2016, doi: 10.1016/j.powtec.2015.10.035.
- [17] H. Chen, Q. Wei, S. Wen, Z. Li, et Y. Shi, « Flow behavior of powder particles in layering process of selective laser melting: Numerical modeling and experimental verification based on discrete element method », *International Journal of Machine Tools and Manufacture*, vol. 123, p. 146-159, déc. 2017, doi: 10.1016/j.ijmachtools.2017.08.004.
- [18] A. L. Maximenko, « Modeling of effect of powder spreading on green body dimensional accuracy in additive manufacturing by binder jetting », *Powder Technology*, p. 9, 2021.
- [19] Y. M. Fouda, « A DEM study of powder spreading in additive layer manufacturing », *Granular Matter*, p. 18, 2019.
- [20] L. Wang, A. Yu, E. Li, H. Shen, et Z. Zhou, « Effects of spreader geometry on powder spreading process in powder bed additive manufacturing », *Powder Technology*, vol. 384, p. 211-222, mai 2021, doi: 10.1016/j.powtec.2021.02.022.
- [21] S. Haeri, « Optimisation of blade type spreaders for powder bed preparation in Additive Manufacturing using DEM simulations », *Powder Technology*, vol. 321, p. 94-104, nov. 2017, doi: 10.1016/j.powtec.2017.08.011.
- [22] *Altair EDEM*. Available at: <https://www.altair.com/edem/>